physica status solidi

pss

www.interscience.wiley.com

reprints

www.pss-rapid.com

www.pss-c.com

www.pss-b.com

www.pss-a.com

WILEY-VCH

REPRINT

Phys. Status Solidi B **247**, No. 8, 1849–1857 (2010) / **DOI** 10.1002/pssb.200983843

physica status solidi b
www.pss-b.com
basic solid state physics

Modification of response properties of the Be(0001) surface upon adsorption of a potassium monolayer: An *ab initio* calculation

V. M. Silkin*,[1,2,3], E. V. Chulkov[1,2,4], J. P. Echeverry[1,2], and P. M. Echenique,[1,2,4]**

[1] Donostia International Physics Center (DIPC), Paseo de Manuel Lardizabal 4, 20018 San Sebastián, Basque Country, Spain
[2] Departamento de Física de Materiales, Facultad de Ciencias Químicas, Universidad del País Vasco, Apto. 1072, 20080 San Sebastián, Basque Country, Spain
[3] IKERBASQUE, Basque Foundation for Science, 48011 Bilbao, Basque Country, Spain
[4] Centro de Física de Materiales (CFM), Materials Physics Center (MPC), Centro Mixto CSIC-UPV/EHU, Edificio Korta, Avenida de Tolosa 72, 20018 San Sebastián, Basque Country, Spain

Received 10 December 2009, revised 23 February 2010, accepted 23 February 2010
Published online 30 June 2010

Keywords adsorbed K monolayers, density functional theory, plasmon excitations, surface states

* Corresponding author: e-mail waxslavs@sc.ehu.es, Phone: +34 943 018 284, Fax: +34 943 015 600
** e-mail wapetlap@sc.ehu.es, Phone: +34 943 015 963, Fax: +34 943 015 600

Collective electronic excitations associated with a potassium monolayer (1 ML) on a Be(0001) substrate are studied using *ab initio* evaluations of the surface response function with the use of energies and wave functions obtained from the self-consistent pseudopotential calculations. The plasmon dispersion relations as well as real and imaginary parts of the dynamical induced charge density oscillations are presented. Comparison of the collective modes of the 1 ML K/Be(0001) system with that of a clean Be(0001) surface is given. It is shown that the K monolayer adsorption leads to appearance, additionally to the conventional surface plasmon of a clean Be surface, of a low-energy mode with characteristic acoustic-like dispersion in the 0–2 eV energy range. The existence of this mode owes to the presence of a K-induced quantum-well-state band whose wave function is strongly localized in the K adlayer. Also we observe a K-derived multipole plasmon with energy around 3 eV. Some other modifications in the Be surface plasmon properties upon K adsorption are discussed as well.

1 Introduction The study of electronic excitations in thin adsorbed alkali metal layers was an active topic for more than four decades [1–23]. These systems are of interest because they show variety of phenomena such as work function changes, metal-insulator transitions, and surface reconstruction. In particular, they allow to investigate in great details the evolution of various basic physical properties of metal surfaces by changing the alkali adatom coverage. Thus the change in the screening properties (in particular, the strong non-locality of the screened interaction) at the surfaces in general [24] and specifically caused by the presence of surface states [25] affects many properties like dynamics of excited states [26] or energy loss of charged particles [27–29]. Also it was investigated in great details how, additionally to the substrate surface [30] and multipole [31] plasmons, the collective modes appear in overlayer of one-monolayer coverage and how these modes evolve with the increase of the adlayer thickness [32–34].

In the microscopic treatment of the electronic excitations in these systems [35–39] a so-called "jellium" model [40] was widely employed to greatly simplify the calculations. At the beginning the adsorbate systems where considered within the two-step jellium model for the description of both adsorbates and substrate [34]. Later on, a method that combines the full three-dimensional (3D) treatment of the adlayers atomic structure and the jellium model for the description of the substrate electronic structure was developed [33, 41–43]. Hence, this approach does not remove important intrinsic limitations of the jellium model in the proper description of the electronic structure of

adsorbate-covered surfaces. The main problem stems from the fact that the jellium model does not allow the appearance of an energy gap in the projected bulk electronic structure and, respectively, surface electronic states whose wave function is linked to the surface [44, 45]. At the same time, many metal surfaces do possess such kind of energy gaps and electronic surface states residing in these gaps [46]. Similar problem exists in the description of the electronic structure of the metal surfaces coated with adsorbates. In particular, it was observed that at certain adsorbate coverage, the discrete adsorbate-derived energy levels called quantum well states (QWSs) appear [47–49]. In the case of alkali adsorbates these states form bands at the center of the surface Brillouin zone (SBZ) with a quasi-free-electron parabolic-like dispersion. Their wave functions are confined to the alkali-metal adlayer by the vacuum barrier from one side and by a reflecting barrier due to an energy gap in the substrate band structure from the other side. When QWSs are located in the energy gap where the substrate bulk electronic states are not allowed they arise as stationary electronic states. On the contrary, when they reside out of such energy gaps they form surface resonances. Hence when the electronic band structure of the substrate is described within the jellium model in which such energy gaps do not exist, the adsobate-induced quantum states always present in the form of broad resonances.

In the present paper we demonstrate the importance of inclusion of the substrate atomic structure in the description of collective electronic excitations induced by an adlayer. For this study we have chosen the p(2 × 2)K/Be(0001) surface whose electronic band structure was investigated very recently [50]. This system is of special interest because upon alkali adsorption a well-ordered surface crystal structure of K atoms commensurate with the Be atomic structure is formed and the alkali-derived QWS band is located in the wide energy gap of the Be(0001) substrate [50]. Hence this QWS exists as a stationary electronic state despite the energy-band folding effect in the substrate which, in principle, should modify its character to the resonance-like one as it occurs in other alkali-adsorbate systems [50, 51]. Here we show that taking into account the full first-principles surface electronic structure of the entire adsorbate/substrate system is of crucial importance for the description of collective electronic excitations. In particular, we find in p(2 × 2)K/Be(0001), additionally to the previously known adsorbate-derived collective excitations [32, 34], a novel well-defined low-energy collective mode with characteristic sound-like energy dispersion, an analogue of recently reported acoustic surface plasmon on clean metal surfaces [52–54]. Note that possibility of such kind of plasmon in adsorbate systems was recently demonstrated on the Na/Cu(111) surfaces in Refs. [22, 55]. However, in difference to the present work, the Na/Cu(111) electronic structure in those papers was taken into consideration via the use of a one-dimensional (1D) model potential [56].

The outline of the paper is as follows. In Section 2 we describe some details of the *ab initio* procedure of calculation of dynamical response properties of surfaces. In Section 3 the results for the p(2 × 2)K/Be(0001) surface are discussed. Comparison of these results with the clean Be(0001) surface data is given in this section as well. Summary and conclusions are presented in Section 4. We use atomic units ($e^2 = \hbar = m_e = 1$) throughout the paper, unless otherwise is stated.

2 Calculation details The surface collective charge excitations can be traced to the peaks in the imaginary part of the surface response function $g(\boldsymbol{q}_{||},\omega)$ [57, 58] derived from the density-response function of the interacting electron system, $\chi(\boldsymbol{r},\boldsymbol{r}',\omega)$ [59]. The imaginary part of the density-response function for interacting electrons $\chi(\boldsymbol{r},\boldsymbol{r}',\omega)$ accounts for the creation of both collective and single-particle excitations in the many-electron system. This function determines an induced dynamical charge density, ρ^{ind}, in the electron system caused by an external potential $\phi^{\mathrm{ext}}(\boldsymbol{r},\omega)$ as

$$\rho^{\mathrm{ind}}(\boldsymbol{r},\omega) = \int d\boldsymbol{r}'\chi(\boldsymbol{r},\boldsymbol{r}',\omega)\phi^{\mathrm{ext}}(\boldsymbol{r}',\omega). \tag{1}$$

In the framework of time-dependent density-functional theory [59, 60] $\chi(\boldsymbol{r},\boldsymbol{r}',\omega)$ obeys the following Dyson-type equation:

$$\chi(\boldsymbol{r},\boldsymbol{r}',\omega) = \chi^0(\boldsymbol{r},\boldsymbol{r}',\omega) + \int \mathrm{d}\boldsymbol{r}_1 \int \mathrm{d}\boldsymbol{r}_2 \chi^0(\boldsymbol{r},\boldsymbol{r}',\omega) \times [\upsilon(\boldsymbol{r}_1,\boldsymbol{r}_2) + f^{\mathrm{xc}}(\boldsymbol{r}_1,\boldsymbol{r}_2,\omega)]\chi(\boldsymbol{r}_2,\boldsymbol{r}',\omega). \tag{2}$$

Here, υ is the bare Coulomb potential and f^{xc} accounts for dynamical exchange-correlation effects. In present work we employ a so-called random-phase approximation when $f^{\mathrm{xc}} = 0$. The density-response function for non-interacting electrons, $\chi^0(\boldsymbol{r},\boldsymbol{r}',\omega)$, is defined as

$$\chi^0(\boldsymbol{r},\boldsymbol{r}',\omega) = \frac{2}{\Omega}\sum_{i,j}(f_i - f_j)\frac{\psi_i(\boldsymbol{r})\psi_j^*(\boldsymbol{r})\psi_j(\boldsymbol{r}')\psi_i^*(\boldsymbol{r}')}{\varepsilon_i - \varepsilon_j + \omega + \mathrm{i}\eta}. \tag{3}$$

Here, factor 2 accounts for spin, Ω the normalization volume, f_i are Fermi-Dirac occupation factors, η is the positive infinitesimal. One-particle energies ε_i and wave-functions ψ_i were calculated in the framework of the local-density approximation [61, 62] with the use of the exchange-correlation potential in the Ceperley-Alder form [63, 64]. Present calculations were performed with the use of repeated-slab geometry, i.e., a semi-infinite solid is represented by slabs of finite thickness separated by vacuum intervals in the direction perpendicular to the surface. This geometry allows us to use the Fourier expansion in all three spatial directions for each calculated quantity. In this case Eq. (2) is transformed into the matrix equation

$$\chi_{GG'}(\boldsymbol{q}_{||},\omega) = \chi^0_{GG'}(\boldsymbol{q}_{||},\omega) + \sum_{G_1,G_2}\chi^0_{GG_1}(\boldsymbol{q}_{||},\omega)[\upsilon_{G_1G_2}(\boldsymbol{q}_{||}) + f^{\mathrm{xc}}_{G_1G_2}(\boldsymbol{q}_{||},\omega)]\chi_{G_2G'}(\boldsymbol{q}_{||},\omega). \tag{4}$$

Here $\boldsymbol{q}_{||}$ is the 2D momentum in the plane parallel to the surface and $\boldsymbol{G}$'s are the 3D reciprocal lattice vectors. Consequently, going on from the real to reciprocal space, χ^0 of Eq. (3) converts into the matrix whose elements are calculated according to

$$\chi^0_{GG'}(\boldsymbol{q}_{||},\omega) = \frac{2}{\Omega}\sum_{\boldsymbol{k}_{||}}^{\mathrm{SBZ}}\sum_{n,n'}\frac{(f_{n\boldsymbol{k}_{||}} - f_{n'\boldsymbol{k}_{||}+\boldsymbol{q}_{||}})}{\varepsilon_{n\boldsymbol{k}_{||}} - \varepsilon_{n'\boldsymbol{k}_{||}+\boldsymbol{q}_{||}} + \omega + \mathrm{i}\eta} \times \left\langle \psi_{n\boldsymbol{k}_{||}} \middle| \mathrm{e}^{-\mathrm{i}(\boldsymbol{q}_{||}+\boldsymbol{G})\boldsymbol{r}} \middle| \psi_{n'\boldsymbol{k}_{||}+\boldsymbol{q}_{||}} \right\rangle \times \left\langle \psi_{n'\boldsymbol{k}_{||}+\boldsymbol{q}_{||}} \middle| \mathrm{e}^{\mathrm{i}(\boldsymbol{q}_{||}+\boldsymbol{G}')\boldsymbol{r}} \middle| \psi_{n\boldsymbol{k}_{||}} \right\rangle, \quad (5)$$

where the sums over n and n' run over band structure for wave vectors $\boldsymbol{k}_{||}$ in the SBZ.

Here we evaluate the excitation spectra of the p(2 × 2)K/Be(0001) surface employing an approach which incorporates in the calculations of $\chi(\boldsymbol{r},\boldsymbol{r}',\omega)$ the full 3D electronic band structure obtained from the *ab initio* pseudopotential method similar to as it was done for clean Mg(0001) and Be(0001) surfaces in Ref. [65, 66], adsorbed linear atomic chains [67, 68], and free-standing metal monolayers [69, 70]. In the present work the *ab initio* electronic structure of the p(2 × 2)K/Be(0001) surface was calculated with the use of norm-conserving pseudopotential [71] and expanding wave functions $\psi_{n\boldsymbol{k}_{||}}(\boldsymbol{r})$ in a plane-wave basis up to the energy cut-off of 20 Ry. The number of Be atomic layers was chosen to be equal 16 and vacuum region corresponds to 10 Be interlayer spacings. Hence the unit cell contains 64 Be and 2 K atoms. The Be lattice parameters and positions of K adatoms were taken from Ref. [50]. The calculation of $\chi^0_{GG'}$ was performed over the 30 × 30 special $\boldsymbol{k}_{||}$-point set in the p(2 × 2)K/Be(0001) SBZ with inclusion of all one-particle electronic states up to energy of 50 eV above the Fermi level. In the case of the clean Be(0001) surface calculations we employed a slab consisting of 24 atomic layers [72] and lattice parameters used in Ref. [62]. A 108 × 108 special $\boldsymbol{k}_{||}$-point set for the summation over the SBZ in Eq. (5) was used. Further details of evaluation of $\chi^0_{GG'}$ matrices within the *ab initio* approach can be found elsewhere [65, 73].

The information about surface collective charge density excitations we obtain from the peaks of the imaginary part of the surface response function $g(\boldsymbol{q}_{||},\omega)$ defined as [57, 58, 65]

$$g(\boldsymbol{q}_{||},\omega) = \int \mathrm{d}\boldsymbol{r}\rho^{\mathrm{ind}}(\boldsymbol{r},\omega)\mathrm{e}^{\boldsymbol{q}_{||}z}, \quad (6)$$

where $\rho^{\mathrm{ind}}(\boldsymbol{r},\omega)$ is the charge density induced at the crystal surface by an external potential in the form

$$\phi^{\mathrm{ext}}(\boldsymbol{r},\omega) = -\frac{2\pi}{q_{||}}\mathrm{e}^{\boldsymbol{q}_{||}z}\mathrm{e}^{\mathrm{i}\boldsymbol{q}_{||}\boldsymbol{r}_{||}}\mathrm{e}^{-\mathrm{i}\omega t}. \quad (7)$$

The final expression for $g(\boldsymbol{q}_{||},\omega)$ used in the numerical calculations [65] is the following

$$g(q_{||},\omega) = -\frac{2\pi}{q_{||}}\sum_{\boldsymbol{G},\boldsymbol{G}'}\chi_{\boldsymbol{G}\boldsymbol{G}'}(q_{||},\omega)\delta_{\boldsymbol{G}_{||}0}\delta_{\boldsymbol{G}_{||}'0}\mathrm{e}^{q_{||}(z+z')}. \quad (8)$$

This expression for $g(\boldsymbol{q}_{||},\omega)$ suggests that when in the system the local field effects [74, 75] are not important in the plane parallel to the surface, matrix $\chi^0_{GG'}$ and, subsequently, $\chi_{GG'}$, can be evaluated considering the reciprocal lattice vectors with zero lateral components only, i.e., those with $\boldsymbol{G}_{||} = \boldsymbol{G}_{||}{}' = 0$ (here we use definition $\boldsymbol{G} \equiv \{\boldsymbol{G}_{||}, \boldsymbol{G}_z\}$). Indeed the unimportance of these effects was demonstrated in the case of a clean Mg(0001) surface [64]. As this allows drastically reduce the computational time we apply the same approach in the case of the p(2 × 2)K/Be(0001) surface as well.

3 Calculation results The calculated *ab initio* band structure of the p(2 × 2)K/Be(0001) surface along symmetry directions of the SBZ is presented in Fig. 1. From comparison with the clean Be(0001) surface electronic structure (it can be found, e.g., in Ref. [76]) one can see that adsorption of the K monolayer introduces strong modifications. First, the surface bands of the clean Be(0001) surface become downshifted in energy in p(2 × 2)K/Be(0001) [50] transforming into the subsurface states as it occurs in other systems [77–80]. Due to reduction of the SBZ size these states are back-folded at new zone boundaries. Second, additionally to the Be-substrate-originated surface bands, a partly occupied K-derived energy band residing in a wide projected energy gap around the SBZ center, i.e., a QWS band, appears. This is in stark contrast with the prediction of

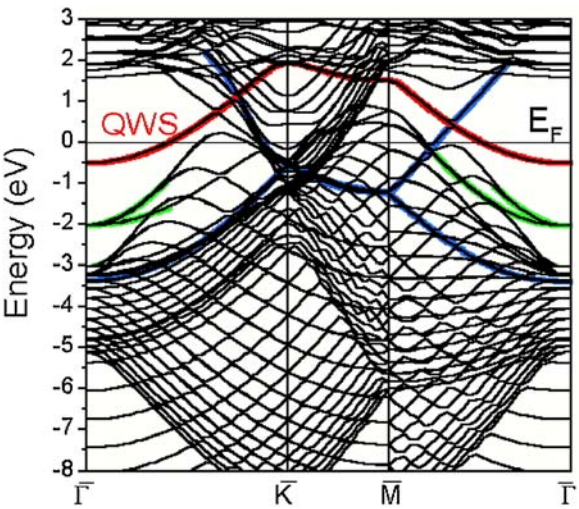

Figure 1 (online color at: www.pss-b.com) *Ab initio* band structure for the p(2 × 2)K/Be(0001) surface along symmetry directions of the SBZ. Red color thick line highlights the K-induced quantum well state (QWS) band dispersion whereas other colored thick lines show Be-substrate-originated back-folded subsurface states. The zero energy corresponds to the Fermi level, E_{F}.

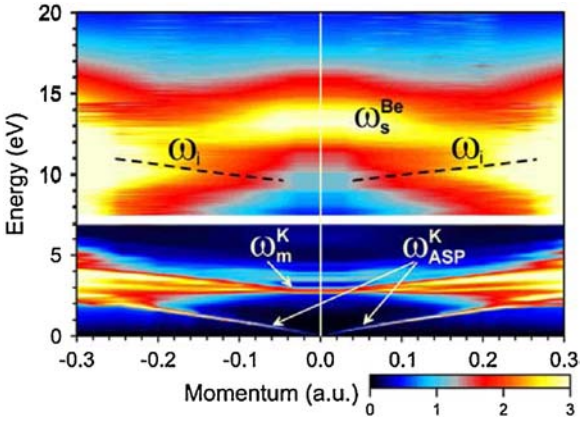

Figure 2 (online color at: www.pss-b.com) Calculated surface-loss function, $\mathrm{Im}[g(q_{||},\omega)]$, for the p(2 × 2)K/Be(0001) surface as a function of energy ω and 2D momentum $\boldsymbol{q}_{||}$ along two symmetry directions of the SBZ. Positive (negative) $q_{||}$ values stand for the $\overline{\Gamma}\,\overline{M}$ $\left(\overline{\Gamma}\,\overline{K}\right)$ direction. The data in upper and lower panels were obtained when origins of the z coordinate in integrations of Eqs. (1) and (6) are placed at the Be crystal border and 3.28 a. u. above the K adlayer position, respectively. Peaks corresponding to the K-derived acoustic surface plasmon $\left(\omega_{\mathrm{ASP}}^{\mathrm{K}}\right)$, multipole plasmon $\left(\omega_{\mathrm{m}}^{\mathrm{K}}\right)$, and Be surface plasmon $\left(\omega_{\mathrm{s}}^{\mathrm{Be}}\right)$ are shown by the corresponding symbols. The dashed lines highlight dispersion of an additional peak, ω_{i}. At small momenta the data for the surface plasmon are distorted due to the finite-thickness-slab effect [30].

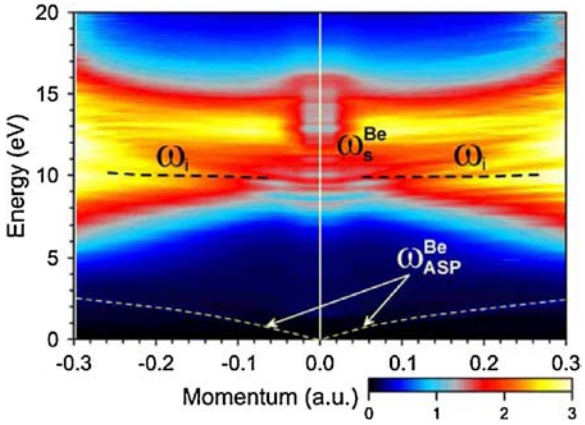

Figure 3 (online color at: www.pss-b.com) Calculated surface-loss function, $\mathrm{Im}[g(q_{||},\omega)]$, for the clean Be(0001) surface as a function of energy ω and 2D momentum $\boldsymbol{q}_{||}$ along two symmetry directions in the SBZ. Positive (negative) $q_{||}$ values stand for the $\overline{\Gamma}\,\overline{M}$ $\left(\overline{\Gamma}\,\overline{K}\right)$ direction. Origins of the z coordinate in integrations of Eqs. (1) and (6) are placed at the Be crystal border. The peaks corresponding to the Be acoustic surface plasmon $\left(\omega_{\mathrm{ASP}}^{\mathrm{Be}}\right)$ and surface plasmon $\left(\omega_{\mathrm{s}}^{\mathrm{Be}}\right)$ are denoted by the corresponding symbols. The dashed lines highlight dispersion of an additional peak, ω_{i} [66]. At small momenta the data for the surface plasmon are distorted due to the finite-thickness-slab effect [30].

the jellium model which does not allow selection of any separate quantum state linked to the K monolayer [81]. The energy position of this band at the $\overline{\Gamma}$ point and its quasiparabolic dispersion is in good agreement with other *ab initio* calculation and experimental photoemission data [50]. Location of this QWS band in the wide energy gap results in almost complete localization of its charge density in the K monolayer [50]. As is shown below this produces qualitatively different excitation spectra obtained from the *ab initio* and jellium models.

The calculated surface loss function, $\mathrm{Im}[g(\boldsymbol{q}_{||},\omega)]$, for the p(2 × 2)K/Be(0001) surface along two symmetry directions is shown in Fig. 2. From comparison with the results for the clean Be(0001) surface presented in Fig. 3 one can observe dramatic modifications in the excitation spectra upon the K monolayer adsorption. The most prominent effect is observed in the low-energy region. Thus instead of the single dispersing peak $\omega_{\mathrm{ASP}}^{\mathrm{Be}}$ in Fig. 3 corresponding to the acoustic surface plasmon of the clean Be(0001) surface [52, 54], in the case of p(2 × 2)K/Be(0001) two dominant features arise at these energies. In the 0–2 eV range a sharp peak $\omega_{\mathrm{ASP}}^{\mathrm{K}}$ with characteristic sound-like dispersion at small momenta is clearly seen in Fig. 2. In Fig. 4 we compare $\mathrm{Im}[g(\boldsymbol{q}_{||},\omega)]$ at $q_{||} = 0.05\,\mathrm{a.u.}^{-1}$ along the $\overline{\Gamma}\,\overline{K}$ direction for both these surfaces, where one can appreciate the magnitude and sharpness of the $\omega_{\mathrm{ASP}}^{\mathrm{K}}$ peak in the case of p(2 ×2)K/Be(0001). This peak corresponds to the acoustic surface plasmon and owes to the presence of the K-derived QWS band. In Fig. 5 which presents the calculated induced charge density, $\rho^{\mathrm{ind}}(z,\boldsymbol{q}_{||},\omega)$, at the same momentum one can clearly see how the charge density oscillations corresponding to the $\omega_{\mathrm{ASP}}^{\mathrm{K}}$ mode are strongly confined to the K monolayer and the adjusted Be region in concert with the strong localization of the QWS charge density [50]. In Fig. 5 one can further observe the dipolar character of this mode in the direction perpendicular to the surface, i.e., it corresponds to the out-of-phase collective charge density oscillations

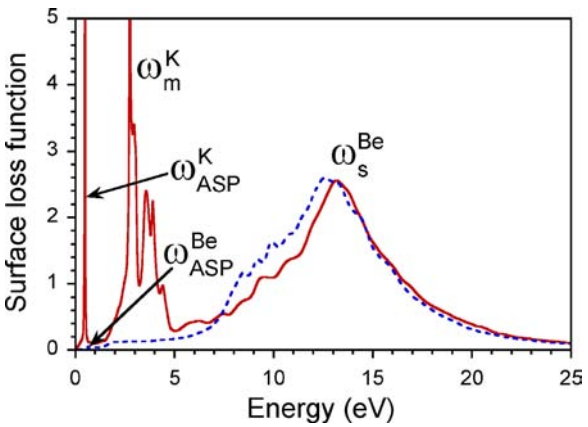

Figure 4 (online color at: www.pss-b.com) Calculated surface-loss function, $\mathrm{Im}[g(q_{||},\omega)]$, for the p(2 × 2)K/Be(0001) (solid red line) and the clean Be(0001) (dashed blue line) surfaces at $q_{||} \equiv |\boldsymbol{q}_{||}| = 0.05\,\mathrm{a.u.}^{-1}$ along the $\overline{\Gamma}\,\overline{K}$ symmetry direction of the SBZ. Both sets of the data are obtained when $z = 0$ is placed at the edge of the Be crystal. Note that the peak $\omega_{\mathrm{ASP}}^{\mathrm{Be}}$ corresponding to the acoustic surface plasmon in the case of the Be(0001) surface is hardly visible on the scale of the figure.

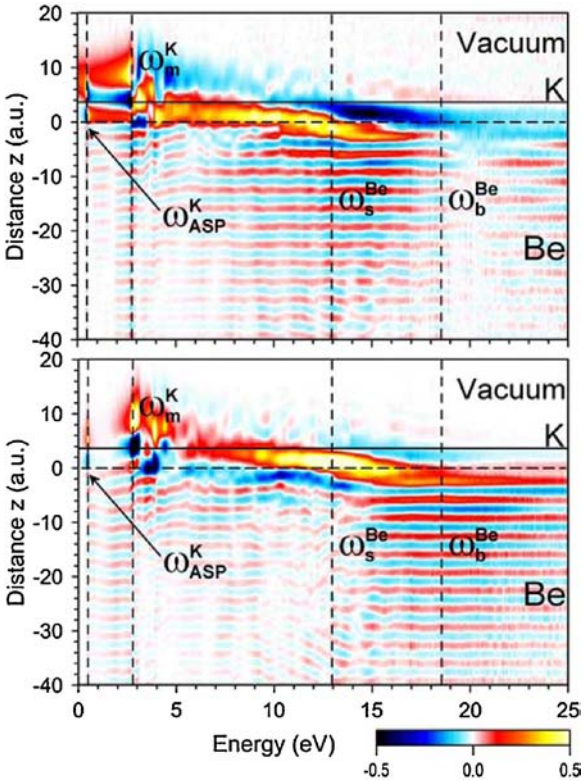

Figure 5 (online color at: www.pss-b.com) p(2 × 2)K/Be(0001) surface: Real (top panel) and imaginary (bottom panel) parts of the laterally averaged induced density, $\rho^{\mathrm{ind}}(z, q_{||}, \omega)$, calculated at $q_{||} \equiv |\boldsymbol{q}_{||}| = 0.05$ a.u.$^{-1}$ along the $\overline{\Gamma}\,\overline{K}$ symmetry direction of the SBZ according to Eq. (1) for ϕ^{ext} in the form of Eq. (8) as a function of energy ω and distance z perpendicular to the surface. The energy positions of the dominant modes are shown by vertical dashed lines and marked by the corresponding symbols. Horizontal solid line denotes position of the K adlayer. The coordinate z is measured from the edge of the Be crystal shown by horizontal dashed line.

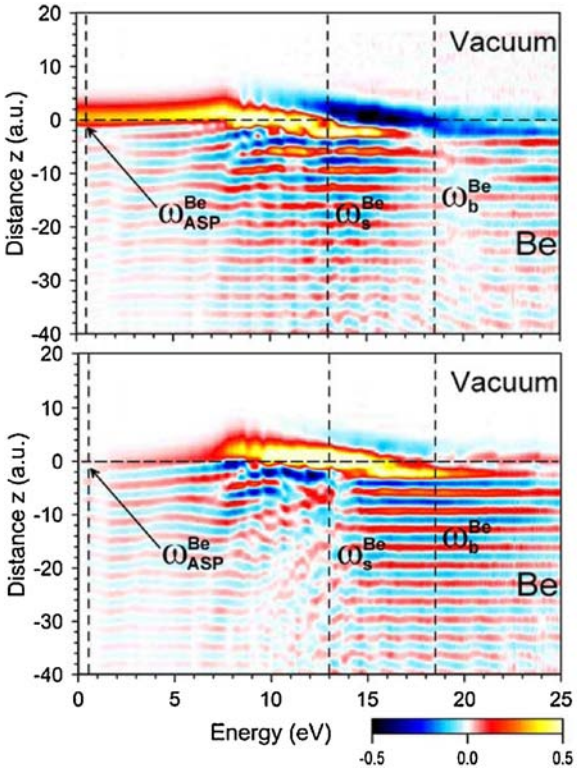

Figure 6 (online color at: www.pss-b.com) Clean Be(0001) surface: Real (top panel) and imaginary (bottom panel) parts of the laterally averaged induced density, $\rho^{\mathrm{ind}}(z, q_{||}, \omega)$, calculated at $q_{||} \equiv |\boldsymbol{q}_{||}| = 0.05$ a.u.$^{-1}$ along the $\overline{\Gamma}\,\overline{K}$ symmetry direction of the SBZ according to Eq. (1) for ϕ^{ext} in the form of Eq. (8) as a function of energy ω and distance z perpendicular to the surface. The energy positions of the dominant modes are shown by vertical dashed lines and marked by the corresponding symbols. The coordinate z is measured from the edge of the Be crystal shown by horizontal dashed line.

between the carriers in the QWS band and the Be substrate electronic system. In this case, a role of a subsystem with slow carriers at the Fermi level [53] is played by the QWS band. Note a very pronounced character of the peak corresponding to the $\omega_{\mathrm{ASP}}^{\mathrm{K}}$ mode in the case of the p(2 × 2)K/Be(0001) surface in comparison with the corresponding mode on the clean Be(0001) surface (see Fig. 6).

This fact can be explained by the stronger spatial decoupling of the QWS wave function from the Be electronic sytem in comparison with the $\overline{\Gamma}$ surface state on the clean Be(0001) surface (a subsystem with slow carriers on this surface) [50]. Figure 2 shows that the $\omega_{\mathrm{ASP}}^{\mathrm{K}}$ mode has quasi-linear dispersion in both directions up to $q_{||} \approx 0.2$ a.u.$^{-1}$ and can clearly be resolved up to $q_{||} \approx 0.3$ a.u.$^{-1}$ where it merges with the broad and almost non-dispersing peak structure. The initial slope of the acoustic surface plasmon $\omega_{\mathrm{ASP}}^{\mathrm{K}}$ dispersion in p(2 × 2)K/Be(0001) is lower in comparison with the similar mode on the Be(0001) surface in accordance with the smaller Fermi velocity v_F in the QWS band (0.2 a.u.) in comparison with the calculated value $v_F = 0.4$ a.u. for the dominant $\overline{\Gamma}$ surface state on Be(0001) [50, 76]. It is interesting to note that we do not observe in Fig. 2 any signature of acoustic surface plasmon related to the dominant $\overline{\Gamma}$ subsurface state (highlighted by blue line in Fig. 1), which gives origin for the $\omega_{\mathrm{ASP}}^{\mathrm{Be}}$ plasmon on the clean Be(0001) surface [52, 54]. A possible explanation for this may be that the K-derived QWS efficiently screens this subsurface state from the external electric field on the vacuum side.

Another salient peak structure in Fig. 2 is observed at energies around $\omega \sim 3$ eV. At small momenta an almost non-dispersing sharp peak $\omega_{\mathrm{m}}^{\mathrm{K}}$ is seen at $\omega = 2.7$ eV which can be attributed to the multipole plasmon mode of the K adlayer. The multipole character of this mode and its strong confinement to the K adlayer is seen in the charge density distribution of Fig. 5. The charge density corresponding to this mode expands in vacuum up distances as far as 15 a.u. from the Be substrate border, i.e., fairly coinciding with the spatial expansion of the QWS charge density [50]. In difference to the jellium model predictions [81], at small momenta the *ab initio* calculation gives the $\omega_{\mathrm{m}}^{\mathrm{K}}$ mode as a

narrow sharp peak (see Figs. 2 and 4). Upon momentum increase in both directions, the ω_m^K peak experiences a slight upward dispersion with gradual increasing of its width. At $q_{||} \approx 0.3$ a.u.$^{-1}$ it forms with the ω_{ASP}^K mode a broad mixed peak structure. Interestingly, in Fig. 5 one can see that at energies close to ω_m^K the screening ability of the p(2 × 2)K/Be(0001) surface is significantly reduced and charge oscillations with notable amplitude can penetrate deeply inside the Be substrate.

In Fig. 2 some additional peaks can be seen in the p(2 × 2)K/Be(0001) surface loss function in the 3.5–4.5 eV energy range at small momenta (see Fig. 4 as well). We attribute these peaks to the numerous interband transitions in the p(2 × 2)K/Be(0001) system. One kind of such transitions may be likely those between the Be-originated subsurface states and the K-derived QWS band. For example, in Fig. 5 it is seen that the penetration of the charge density oscillations at the $\omega = 3.6$ eV (which corresponds to a local peak in $\mathrm{Im}[g(\boldsymbol{q}_{||}, \omega)]$) is the same as the penetration depth for the Be subsurface states [50], whereas its expansion in the vacuum is in concert with the K QWS wave function localization [50].

In the upper energy region of Figs. 2 and 4, the surface loss function of the p(2 × 2)K/Be(0001) surface at small momenta is dominated by a broad ω_s^{Be} peak corresponding to the conventional surface plasmon of the Be substrate. At these $\boldsymbol{q}_{||}$'s, the energy position and width of the ω_s^{Be} peak fairly well coincide with that on clean Be(0001) surface of Fig. 3. Nevertheless, some differences can be detected between these two systems. Thus as is seen in Fig. 4 the intensity of the ω_s^{Be} peak in p(2 × 2)K/Be(0001) on the low-energy side is lower in comparison with the Be(0001) case. Moreover, in Fig. 2 for p(2 × 2)K/Be(0001) one can note that, upon momentum increase, instead of small positive dispersion of the ω_s^{Be} peak on Be(0001) [66] (Fig. 3), it experiences notable negative dispersion up to $q_{||} \approx 0.24$ a.u.$^{-1}$, where it reaches a minimum at $\omega \sim 11$ eV (see Fig. 7) and does not possess a positive dispersion at the all momenta studied. On the other hand, another slightly dispersing ω_i peak around $\omega \sim 10$ eV (highlighted by dashed line in Fig. 2) can be clearly seen in the surface loss function of p(2 × 2)K/Be(0001). Similarly to the clean Be(0001) surface case (Fig. 3), this feature appears at some finite values of momentum and becomes a dominant feature at large momenta. Figure 7 demonstrates significantly more pronounced redistribution of the absorption strength from the ∼13 eV energy region to the lower energy part in $\mathrm{Im}[g(\boldsymbol{q}_{||}, \omega)]$ for p(2 × 2)K/Be(0001) in comparison with the clean Be(0001) surface. Induced charge density distributions in Figs. 5 and 6 confirm similarity of this in the both studied systems. Nevertheless, close inspection of these figures reveals some differences, which can be attributed to the differences in the electronic structure in both systems. Thus in ρ^{ind} of Figs. 5 and 6 notable differences in the 7–13 energy range can be detected below the top Be atomic layer.

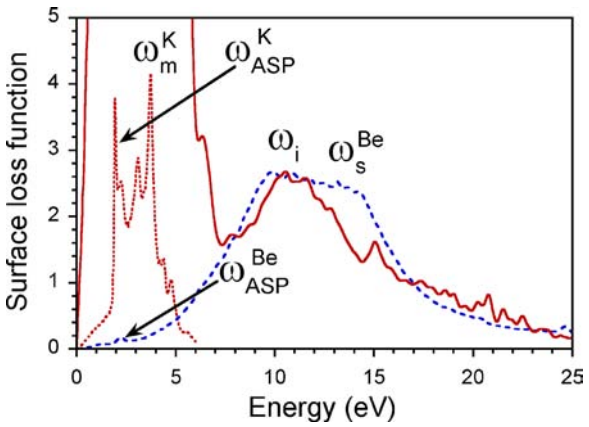

Figure 7 (online color at: www.pss-b.com) Surface-loss function, $\mathrm{Im}[g(q_{||}, \omega)]$, for the p(2 × 2)K/Be(0001) (solid red line) and the clean Be(0001) (dashed blue line) surfaces calculated at $q_{||} \equiv |\boldsymbol{q}_{||}| = 0.24$ a.u.$^{-1}$ along the $\overline{\Gamma}\,\overline{K}$ symmetry direction of the SBZ. Both sets of data are obtained when the $z = 0$ position is placed at the edge of the Be crystal. In the low-energy region dotted red line shows the same as solid red line divided by a factor 30.

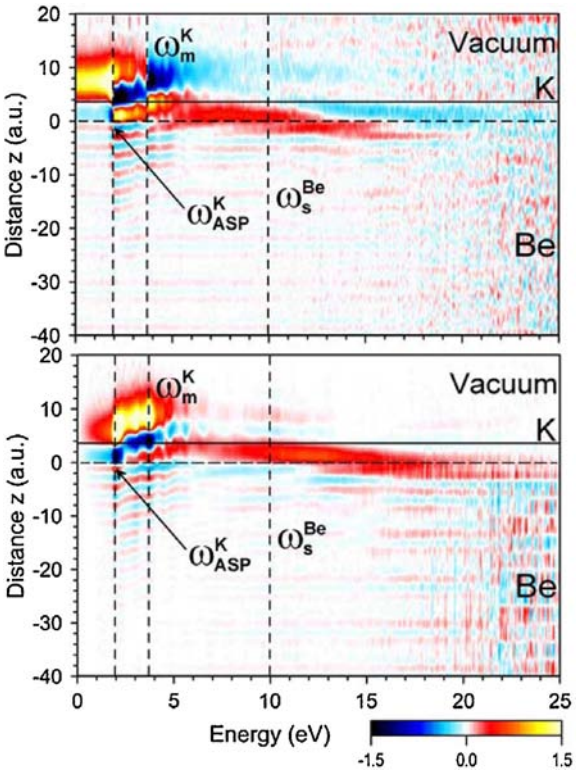

Figure 8 (online color at: www.pss-b.com) p(2 × 2)K/Be(0001)surface: Real (top panel) and imaginary (bottom panel) parts of the laterally averaged induced density, $\rho^{ind}(z, q_{||}, \omega)$, calculated at $q_{||} \equiv |\boldsymbol{q}_{||}| = 0.24$ a.u.$^{-1}$ along the $\overline{\Gamma}\,\overline{K}$ symmetry direction of the SBZ according to Eq. (1) for ϕ^{ext} in the form of Eq. (8) as a function of energy ω and distance z perpendicular to the surface. The energy positions of the dominant modes are shown by vertical dashed lines and marked by the corresponding symbols. Horizontal solid line denotes position of the K adlayer. The coordinate z is measured from the edge of the Be crystal shown by horizontal dashed line.

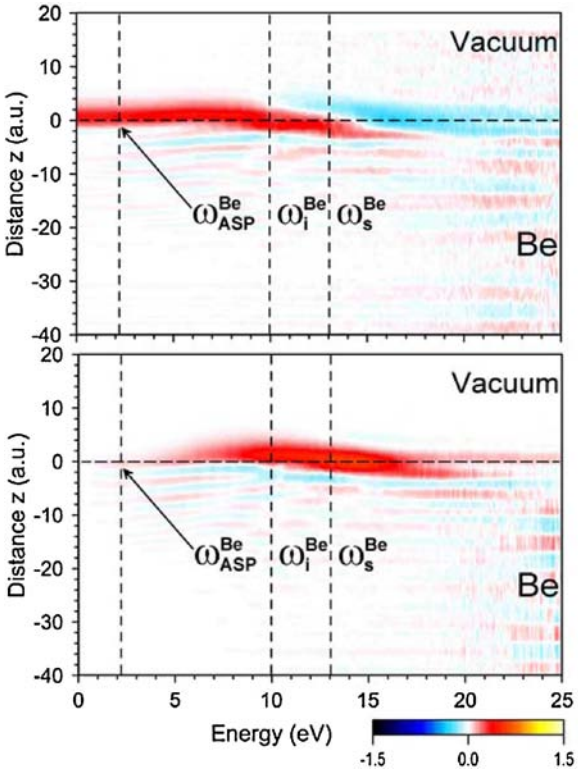

Figure 9 (online color at: www.pss-b.com) Clean Be(0001) surface: Real (top panel) and imaginary (bottom panel) parts of the laterally averaged induced density, $\rho^{\mathrm{ind}}(z, q_{||}, \omega)$, calculated at $q_{||} \equiv |\boldsymbol{q}_{||}| = 0.24\,\mathrm{a.u.}^{-1}$ along the $\overline{\Gamma}\,\overline{K}$ symmetry direction of the SBZ according to Eq. (1) for ϕ^{ext} in the form of Eq. (8) as a function of energy ω and distance z perpendicular to the surface. The energy positions of the dominant modes are shown by vertical dashed lines and marked by the corresponding symbols. The coordinate z is measured from the edge of the Be crystal shown by horizontal dashed line.

It is interesting to address completely different behavior of ρ^{ind} in the interior of the Be substrate at energies in vicinity of the Be plasmon energy, $\omega_{\mathrm{b}}^{\mathrm{Be}}$, in comparison with that obtained within the jellium model [81]. In particular, instead of strong energy oscillations of $\rho^{\mathrm{ind}}(z, \boldsymbol{q}_{||}, \omega)$ at a given distance z for energies $\omega > \omega_{\mathrm{b}}^{\mathrm{Be}}$ in the jellium model, the *ab initio* $\rho^{\mathrm{ind}}(z, \boldsymbol{q}_{||}, \omega)$ in Figs. 5 and 6 is almost energy independent for these energies. We relate this behavior to the large width of the Be bulk plasmon peak obtained in the *ab initio* calculations because of the strong band structure effects [82], which is in close agreement with experiment [83, 84].

Figures 2 and 7 demonstrate how upon momentum increase the relative intensity of the adsorbate-induced features dramatically increases due to stronger confinement of the external electric field in the K adlayer. To demonstrate this effect, Figs. 8 and 9 present $\rho^{\mathrm{ind}}(z, \boldsymbol{q}_{||}, \omega)$ calculated at $q_{||} \approx 0.24\,\mathrm{a.u.}^{-1}$ for the p(2 × 2)K/Be(0001) and Be(0001) surfaces, respectively. Here one can observe how the intensity of the low-energy peaks is greatly enhanced in comparison with the surface plasmon. The z-dependence of the charge density oscillations in Fig. 8 at $\omega_{\mathrm{m}}^{\mathrm{K}}$ is essentially the same as that at smaller momentum of Fig. 5. Even the penetration inside the Be substrate is very similar in Figs. 5 and 8. On the other hand, as is seen in Fig. 7 instead of a two-peak structure in surface loss function of the Be(0001) surface (at ∼10 and ∼13 eV), in p(2 × 2)K/Be(0001) only one clear peak at ∼11 eV exists. From the charge density distribution of Fig. 8, we assign this peak as a Be surface plasmon although some extra oscillations at the region where the K adlayer is located can be observed in ρ^{ind} of Fig. 8 signaling about some effect of the K-induced QWS in shaping of the $\omega_{\mathrm{s}}^{\mathrm{Be}}$ properties at large momenta.

4 Summary and conclusions We have presented results of the surface response function for the p(2 × 2)K/Be(0001) surface performed with full inclusion of the *ab initio* band structure. From comparison with similar results for the clean Be(0001) surface, we have investigated the impact of adsorption of one K ML on the dynamical response properties of this surface. Presented results reveal that the most important effect of deposition of the K monolayer is the appearance of extremely narrow acoustic surface plasmon corresponding to out-of-phase collective charge density oscillations between the carriers in the K QWS and the Be electronic system. We have also found a narrow peak in the surface loss function of p(2 × 2)K/Be(0001) corresponding to a well-defined adsorbate multipole plasmon. The profound impact of the K adsorption on the properties of the Be(0001) surface plasmon dramatically increasing with momentum is demonstrated as well.

Acknowledgements We acknowledge partial support from the University of the Basque Country (grant no. GIC07IT36607), the Departamento de Educación del Gobierno Vasco, and the Spanish Ministerio de Educación y Ciencia (grant no. FIS200766711C0101), and programa CONSOLIDER.

References

[1] A. U. MacRae, K. Müller, J. J. Lander, J. Morrison, and J. C. Phillips, Phys. Rev. Lett. **22**, 1048 (1969).
[2] J. W. Gadzuk, Phys. Rev. B **1**, 1267 (1970).
[3] D. M. Newns, Phys. Lett. A **39**, 341 (1972).
[4] J. E. Inglesfield and E. Wikborg, J. Phys.: Met. **5**, 1706 (1975).
[5] S. A. Lindgren and L. Walldén, Phys. Rev. B **22**, 5967 (1980).
[6] A. Hohfeld, M. Sunjic, and K. Horn, J. Vac. Sci. Technol. A **5**, 679 (1987).
[7] K. Kempa and W. L. Schaich, Solid State Commun. **61**, 357 (1987).
[8] D. Heskett, K.-H. Frank, K. Horn, E. E. Koch, H.-J. Freund, A. Baddorf, K.-D. Tsuei, and E. W. Plummer, Phys. Rev. B **37**, 10387 (1988).
[9] R. Fuchs and W. Ekardt, J. Phys.: Condens. Matter **1**, 4081 (1989).
[10] J. A. Gaspar, A. G. Eguiluz, K.-D. Tsuei, and E. W. Plummer, Phys. Rev. Lett. **67**, 2854 (1991).

[11] W. Plummer, K.-D. Tsuei, and B.-O. Kim, Nucl. Instrum. Methods Phys. Res. B **96**, 448 (1995).
[12] M. Rocca, Surf. Sci. Rep. **22**, 1 (1995).
[13] S. R. Barman, K. Horn, P. Häberle, H. Ishida, and A. Liebsch, Phys. Rev. B **57**, 6662 (1998).
[14] F. Moresco, M. Rocca, T. Hildebrandt, V. Zielasek, and M. Henzler, Europhys. Lett. **43**, 433 (1998).
[15] S. R. Barman, P. Häberle, and K. Horn, Phys. Rev. B **58**, R4285 (1998).
[16] F. Moresco, M. Rocca, T. Hildebrandt, and M. Henzler, Surf. Sci. **424**, 55 (1999).
[17] F. Moresco, M. Rocca, T. Hildebrandt, V. Zielasek, and M. Henzler, Surf. Sci. **424**, 62 (1999).
[18] S. R. Barman, C. Stampfl, P. Häberle, and K. Horn, Phys. Rev. B **61**, 12721 (2000).
[19] S. R. Barman, P. Häberle, K. Horn, J. A. Maytorena, and A. Liebsch, Phys. Rev. Lett. **86**, 5108 (2001).
[20] V. Zielasek, N. Rönitz, M. Henzler, and H. Pfnür, Phys. Rev. Lett. **96**, 196801 (2006).
[21] A. Politano, R. G. Agostino, E. Colavita, V. Formoso, and G. Chiarello, J. Chem. Phys. **126**, 244712 (2007).
[22] V. M. Silkin, M. Quijada, M. G. Vergniory, M. Alducin, A. G. Borisov, R. Díez Muiño, J. I. Juaristi, D. Sánchez-Portal, E. V. Chulkov, and P. M. Echenique, Nucl. Instrum. Methods Phys. Res. B **258**, 72 (2007).
[23] A. Politano, R. G. Agostino, E. Colavita, V. Formoso, and G. Chiarello, J. Nanosci. Nanotechnol. **9**, 3932 (2009).
[24] I. Sarría, J. Osma, E. V. Chulkov, J. M. Ritarke, and P. M. Echenique, Phys. Rev. B **60**, 11795 (1999).
[25] J. Osma, I. Sarría, E. V. Chulkov, J. M. Pitarke, and P. M. Echenique, Phys. Rev. B **59**, 10591 (1999).
[26] E. V. Chulkov, A. G. Borisov, J. P. Gauyacq, D. Sánchez-Portal, V. M. Silkin, V. P. Zhukov, and P. M. Echenique, Chem. Rev. (Washington, DC) **106**, 4160 (2006).
[27] A. Närmann, R. Monreal, P. M. Echenique, F. Flores, W. Heiland, and S. Schubert, Phys. Rev. Lett. **64**, 1601 (1990).
[28] J. I. Juaristi, A. Arnau, P. M. Echenique, C. Auth, and H. Winter, Phys. Rev. Lett. **82**, 1048 (1999).
[29] R. Díez Muiño, A. Arnau, and P. M. Echenique, Nucl. Instrum. Methods Phys. Res. B **98**, 420 (1995).
[30] R. H. Ritchie, Phys. Rev. **106**, 874 (1957).
[31] A. J. Bennett, Phys. Rev. B **1**, 203 (1970).
[32] A. Liebsch, Phys. Rev. Lett. **67**, 2858 (1991).
[33] H. Ishida and A. Liebsch, Phys. Rev. B **45**, 6171 (1992).
[34] A. G. Eguiluz and D. A. Campbell, Phys. Rev. B **31**, 7572 (1985).
[35] P. J. Feibelman, Phys. Rev. B **12**, 1319 (1975).
[36] P. J. Feibelman, Prog. Surf. Sci. **12**, 287 (1982).
[37] A. Liebsch, Phys. Rev. B **36**, 7378 (1987).
[38] A. G. Eguiluz, Phys. Rev. Lett. **51**, 1907 (1983).
[39] A. G. Eguiluz, Phys. Rev. B **31**, 3303 (1985).
[40] N. D. Lang, Phys. Rev. B **4**, 4234 (1971).
[41] H. Ishida and A. Liebsch, Phys. Rev. B **57**, 12550 (1998).
[42] H. Ishida and A. Liebsch, Phys. Rev. B **57**, 12558 (1998).
[43] S. R. Barman, C. Stampfl, P. Häberle, W. Ibañez, Y. Q. Cai, and K. Horn, Phys. Rev. B **64**, 195410 (2001).
[44] I. E. Tamm, Phys. Z. Sowjet. **1**, 733 (1932).
[45] W. Shockley, Phys. Rev. **56**, 317 (1939).
[46] J. E. Inglesfield, Rep. Prog. Phys. **45**, 223 (1982).
[47] S.-Å. Lindgren and L. Walldén, Phys. Rev. Lett. **59**, 3003 (1987).
[48] A. Carlsson, D. Claesson, S.-Å. Lindgren, and L. Walldén, Phys. Rev. Lett. **77**, 346 (1996).
[49] T.-C. Chiang, Surf. Sci. Rep. **39**, 181 (2000).
[50] J. Algdal, T. Balasubramanian, M. Breitholtz, V. Chis, B. Hellsing, S.-Å. Lindgren, and L. Walldén, Phys. Rev. B **78**, 085102 (2008).
[51] C. Corriol, V. M. Silkin, D. Sánchez-Portal, A. Arnau, E. V. Chulkov, P. M. Echenique, T. von Hofe, J. Kliewer, J. Kröger, and R. Berndt, Phys. Rev. Lett. **95**, 176802 (2005).
[52] V. M. Silkin, A. García-Lekue, J. M. Pitarke, E. V. Chulkov, E. Zaremba, and P. M. Echenique, Europhys. Lett. **66**, 260 (2004).
[53] V. M. Silkin, J. M. Pitarke, E. V. Chulkov, and P. M. Echenique, Phys. Rev. B **72**, 115435 (2005).
[54] B. Diaconescu, K. Pohl, L. Vattuone, L. Savio, Ph. Hofmann, V. M. Silkin, J. M. Pitarke, E. V. Chulkov, P. M. Echenique, D. Farías, and M. Rocca, Nature (London) **448**, 57 (2007).
[55] V. M. Silkin, M. Quijada, R. Díez Muiño, E. V. Chulkov, and P. M. Echenique, Surf. Sci. **601**, 4546 (2007).
[56] E. V. Chulkov, J. Kliewer, R. Berndt, V. M. Silkin, B. Hellsing, S. Crampin, and P. M. Echenique, Phys. Rev. B **68**, 195422 (2003).
[57] B. N. J. Persson and E. Zaremba, Phys. Rev. B **31**, 1863 (1985).
[58] A. Liebsch, Electronic Excitations at Metal Surfaces (Plenum Press, New York, 1997).
[59] E. Runge and E. K. U. Gross, Phys. Rev. Lett. **52**, 997 (1984).
[60] E. K. U. Gross and W. Kohn, Adv. Quantum Chem. **21**, 255 (1990).
[61] P. Hohenberg and W. Kohn, Phys. Rev. **136**, B864 (1964).
[62] W. Kohn and L. J. Sham, Phys. Rev. **140**, A1133 (1965).
[63] D. M. Ceperley and B. J. Alder, Phys. Rev. Lett. **45**, 566 (1980).
[64] J. P. Perdew and A. Zunger, Phys. Rev. B **23**, 5048 (1981).
[65] V. M. Silkin, E. V. Chulkov, and P. M. Echenique, Phys. Rev. Lett. **93**, 176801 (2004).
[66] V. M. Silkin, E. V. Chulkov, and P. M. Echenique, Radiat. Eff. Defects Solids **162**, 483 (2007).
[67] J. Yan, Z. Yuan, and S. W. Gao, Phys. Rev. Lett. **98**, 216602 (2007).
[68] J. Yan and S. W. Gao, Phys. Rev. B **78**, 235413 (2008).
[69] A. Bergara, V. M. Silkin, E. V. Chulkov, and P. M. Echenique, Phys. Rev. B **67**, 245402 (2003).
[70] Z. Yuan and S. W. Gao, Comput. Phys. Commun. **180**, 466 (2009).
[71] Y. V. Chulkov, V. M. Silkin, and Y. N. Shirykalov, Phys. Met. Metallogr. **64**, 1 (1987) [Fiz. Met. Metalloved. **64**, 213 (1987)].
[72] We have checked that the results are converged with respect to the vacuum thickness used because we avoid long-range Coulomb interaction between slabs performing the real space integrations in Eq. (2) only for one slab with nearby vacuum regions. On the other hand, at small momenta the surface plasmon properties are strongly dependent on the slab thickness due to the splitting into two slab symmetrical and antisymmetrical modes [30].
[73] V. M. Silkin, J. M. Pitarke, E. V. Chulkov, B. Diaconescu, K. Pohl, L. Vattuone, L. Savio, Ph. Hofmann, D. Farías, M. Rocca, and P. M. Echenique, Phys. Status Solidi A **205**, 1307 (2008).

[74] S. L. Adler, Phys. Rev. **126**, 413 (1962).
[75] N. Wiser, Phys. Rev. **129**, 62 (1963).
[76] E. V. Chulkov, V. M. Silkin, and E. N. Shirykalov, Surf. Sci. **188**, 287 (1987).
[77] E. V. Chulkov and V. M. Silkin, Surf. Sci. **215**, 385 (1989).
[78] C. Stampfl, K. Kambe, R. Fasel, P. Aebi, and M. Scheffler, Phys. Rev. B **57**, 15251 (1998).
[79] J. M. Carlsson and B. Hellsing, Phys. Rev. B **61**, 13973 (2000).
[80] M. Breitholtz, V. Chis, B. Hellsing, S.-Å. Lindgren, and L. Walldén, Phys. Rev. B **75**, 155403 (2007).
[81] J. P. Echeverry, E. V. Chulkov, and V. M. Silkin, Phys. Status Solidi C, submitted (2010), DOI: 10.1002/pssc.200983842.
[82] V. M. Silkin, E. V. Chulkov, and P. M. Echenique, Phys. Rev. B **68**, 205106 (2003).
[83] P. Eisenberger, P. M. Platzman, and K. C. Pandy, Phys. Rev. Lett. **31**, 311 (1973).
[84] W. Schülke, H. Nagasawa, S. Mourikis, and A. Kaprolat, Phys. Rev. B **40**, 12215 (1989).